

Review

Research Progress on Bionic Recognition and Biosensors for the Detection of Biomarkers of Diabetic Nephropathy

Ye Tian ^{1,*}, Lili Gao ^{2,†}, Abubakar Abdussalam ^{3,4}  and Guobao Xu ^{3,4,*} ¹ The College of Civil Engineering, Shenyang Urban Construction University, Shenyang 110167, China² School of Materials Science and Engineering, Shenyang Jianzhu University, Shenyang 110168, China; liligao@sjzu.edu.cn³ State Key Laboratory of Electroanalytical Chemistry, Changchun Institute of Applied Chemistry, Chinese Academy of Sciences, Changchun 130022, China; aasalam@ciac.ac.cn⁴ School of Applied Chemistry and Engineering, University of Science and Technology of China, Hefei 230026, China

* Correspondence: tumugongchengxueyuantian@syucu.edu.cn (Y.T.); guobaoxu@ciac.ac.cn (G.X.)

† These authors contributed equally to this work.

Abstract: Diabetic nephropathy (DN) refers to kidney damage caused by diabetes and is one of the major microvascular complications of diabetes. This disease has a certain degree of concealment in the early stage, with clinical symptoms appearing later and a higher mortality rate. Therefore, the detection of early biomarkers for DN is of great importance in reducing kidney function damage. The common biomarkers for DN mainly include glomerular and tubular lesion markers. At present, clinical diagnosis often uses a combination of multiple indicators and symptoms, and the development of a simple, efficient, and sensitive multi-marker detection platform is particularly important for the early diagnosis of DN. In recent years, with the vigorous development of various biomimetic molecular recognition technologies, biomimetic recognition biosensors (BRBS) have many advantages, such as easy preparation, low cost, high stability, and repeatability under harsh environmental conditions, and have great application potential in the analysis of DN biomarkers. This article reviews the research progress of molecularly imprinted polymers (MIPs) construction technology and aptamers assembly technology developed in the field of biomimetic sensor research in recent years, as well as the detection of DN biomarkers based on BRBS, and prospects for their development.

Keywords: bionic recognition; MIPs; aptamers; diabetic nephropathy; biomarkers



check for updates

Citation: Tian, Y.; Gao, L.; Abdussalam, A.; Xu, G. Research Progress on Bionic Recognition and Biosensors for the Detection of Biomarkers of Diabetic Nephropathy. *Chemosensors* **2023**, *11*, 510. <https://doi.org/10.3390/chemosensors11100510>

Academic Editor: Ambra Giannetti

Received: 12 July 2023

Revised: 6 September 2023

Accepted: 17 September 2023

Published: 22 September 2023



Copyright: © 2023 by the authors. Licensee MDPI, Basel, Switzerland. This article is an open access article distributed under the terms and conditions of the Creative Commons Attribution (CC BY) license (<https://creativecommons.org/licenses/by/4.0/>).

1. Introduction

Diabetic nephropathy (DN) refers to kidney damage caused by diabetes, which is one of the main microvascular complications of diabetes. High blood sugar-induced kidney damage leads to a decrease in the glomerular filtration rate (GFR) and the appearance of symptoms such as proteinuria. The disease has a high mortality rate [1]. Currently, DN has seriously threatened human health and the development of socio-economic progress [2]. According to the classification of DN by Mogensen from Denmark, stage I–II lacks obvious clinical manifestations, stage III begins to show trace albuminuria and GFR may be normal, and it is not until stage IV that there is a persistent and progressively worsening amount of albuminuria accompanied by a decline in GFR, which is difficult to reverse, eventually leading to renal failure. Therefore, early DN is reversible, and if diagnosed and treated with early intervention, the development of nephropathy can be halted or reversed. Hence, early screening and diagnosis are particularly important for DN. The screening of DN mainly follows the standards of the American Diabetes Association (ADA), including albuminuria and GFR. However, a large number of clinical observations have found that 20–50% of chronic kidney disease patients have no albuminuria, and the number of such patients is on the rise [3]. This means that these DN patients without albuminuria will be missed, and will

not receive timely diagnosis and treatment. Therefore, it is of great practical significance to find highly sensitive and specific early biomarkers for DN and establish accurate and convenient detection methods.

So far, several analytical methods have been developed for the detection of biomarkers (urinary albumin, creatinine, cystatin C, homocysteine, vascular endothelial growth factor, epidermal growth factor receptor, mRNA-21, ceruloplasmin, platelet-derived growth factor, etc.) for DN [4–7], including ultra-high performance liquid chromatography (UHPLC), capillary electrophoresis (CE), liquid chromatography-tandem mass spectrometry (LC-MS), radioimmunoassay (RIA), enzyme-linked immunosorbent assay (ELISA), immunoradiometry (IRMA), and electrochemiluminescent immunoassay (ECLI). Although the results of these methods are reliable and accurate, they have many disadvantages, such as large sample sizes, complex instruments, expensive antibodies, long incubation time, and complicated protocols. These limitations restrict their application in real-time detection [8,9]. Therefore, the introduction of rapid, universal, powerful, and high-throughput sensing technologies for early detection of DN has significant social value.

In recent years, researchers have developed a large number of novel biosensors with high specificity and sensitivity [10,11]. Traditional biosensor recognition elements mainly consist of biological molecules with molecular recognition capabilities, such as antibodies, enzymes, nucleic acids, cells, and semi-synthetic receptors based on them. However, they have inherent drawbacks, such as difficulty in preparation, high cost, and poor stability, which greatly limit their application in the analysis of diabetes kidney disease biomarkers. Compared with traditional biosensors, the biomimetic recognition elements of biomimetic recognition biosensors (BRBS), including MIPs and APT, can be synthesized through in vitro preparation methods. This not only effectively avoids the tedious work of bio-receptor preparation using experimental animals but also reduces the batch-to-batch variability of recognition elements, significantly lowering manufacturing costs. The application of BRBS in the electrochemical sensing field has greatly promoted the development of analytical chemistry and electroanalytical chemistry. Among them, molecularly imprinted electrochemical sensors (MIECS) combine the predetermined recognition and specificity of molecular imprinting technique (MIT) with the high sensitivity, easy operation, low cost, and miniaturization advantages of electrochemical technology [12].

MIT is inspired by the “antigen-antibody” theory and prepares MIPs targeted to specific molecules. Currently, most MIPs are made of vinyl organic compounds or acrylic acid as functional monomers, forming through free radical polymerization under the influence of crosslinking agents, initiators, light or heat, etc. MIPs can selectively recognize template molecules (TM) or their analogs mainly because, after removing the TM in the polymer, highly crosslinked polymers retain “empty holes” with multiple active sites that match the size and conformation of the TM. MIPs demonstrate excellent resistance to harsh environmental interference, but there is a possibility of template leakage when analyzing complex samples, especially for trace analysis, the leakage of residual templates directly affects the accuracy of the analysis results. Moreover, the preparation of MIPs becomes difficult due to the poor solubility of certain specific TM. Using a dummy template molecule that has a similar structure or the same functional groups as the template molecule solves this issue, as the 3D cavity structure and interaction sites left by the dummy molecularly imprinted polymer still have some compatibility with the template molecule. Thus, dummy molecular imprinting technology can solve the problems of template leakage, high costs, and difficulties in preparing MIPs due to the poor solubility of certain specific TM [13]. However, the binding sites, shape, and size of the cavities prepared by the dummy template may not completely match the target molecule, which may reduce sensitivity and detection limits. Therefore, the selection of appropriate functional monomers, crosslinking agents, solvents, polymerization conditions, washing conditions, and preparation methods is crucial for obtaining good specific molecular recognition capabilities during the preparation of molecular imprinting membranes. To achieve breakthrough progress in the field of MIT

electrochemical sensing, it is necessary to design and develop better MIP preparation technology strategies.

Research shows that nucleic acid APT are single-stranded RNA or DNA molecules extracted from a library of oligonucleotide ligands through systematic evolution of ligands by exponential enrichment (SELEX) technology. They have advantages such as non-toxicity, ease of preparation, low cost, chemical stability, and high binding efficiency to target molecules [14]. Compared to antibodies, APTs have much lower molecular weight, can recognize subtle structural differences in biomarkers, and are easily dissociable [15]. Furthermore, the shape and length of APT can be controlled and flexibly modified, forming structures with specific physicochemical properties and functions. Research of multifarious adenine-mediated technology (MAMT) suggests that the adsorption capabilities of the four bases of nucleic acid APT to gold follow the order $A > C \geq G > T$ [16]. Among them, adenine has strong adsorption to gold, comparable to Au-S bonds, and Au can even denature the double strands of adenine and thymine. The strong adsorption of adenine to gold electrodes has promising applications in the design of thiol-free APT [17]. Adenine can be used as an anchoring group and density control group to regulate the conformation and grafting density of APT at the sensor interface, reducing the surface density of APT on the electrode with the increase of adenine length. Moreover, adenine preferentially binds to gold atoms, reducing the accessibility of other materials to gold, and significantly hindering the non-specific adsorption of other materials. These aptamer (APT) assembly techniques can be applied to the construction of biosensors.

In recent years, with the development of MIT and APT assembly technology, the application of bionic recognition biosensors in the field of DN biomarker analysis has been effectively expanded. With the discovery of new biomarkers for DN, the development of more efficient, stable, and cost-effective novel biomimetic sensing platforms has significant implications. Not only does it improve our understanding of the pathogenesis of DN and further promote early diagnosis in diabetic nephropathy patients, but it also optimizes the treatment of these patients. Therefore, this article reviews the research progress in the construction of MIPs, APT assembly technology, and the detection of biomarkers for DN based on BRBS in the field of biomimetic sensors in recent years, and forecasts their development.

2. Application of BRBS in the Detection of Diabetic Nephropathy Biomarkers

Early biomarkers of diabetic nephropathy can be divided into glomerular dysfunction markers and tubular dysfunction markers according to the site of lesions. So far, a series of biomarkers have been introduced into the diagnosis of diabetic nephropathy,

2.1. Urinary Albumin

Urinary albumin detection reflects abnormal protein leakage in the kidney and can understand early kidney disease and kidney injury. Pathological increases are seen in diabetic nephropathy, hypertension, and preeclampsia during pregnancy [18]. If the albumin in the urine is in the range of 30–200 mg/L, it belongs to microalbuminuria. Early diabetic nephropathy is a mild increase in urinary albumin excretion (microalbuminuria), which gradually progresses to massive albuminuria and eventually kidney failure, requiring dialysis or kidney transplantation. Up to now, microalbuminuria is still the best non-invasive biomarker for detecting diabetic nephropathy [19].

Zhang [20] successfully constructed a MIP-ECS based on a dual-signal strategy for human serum albumin (HSA) detection in urine (Figure 1). Firstly, the glassy carbon electrode (GE) substrate was modified with AuNPs and polythionine-methylene blue (PTH-MB) sequentially. Then, a dual-functional monomer molecularly imprinted polymer (MIP) was prepared by the electropolymerization method using human serum albumin (HAS) as the TM, HQ, and *o*-phenylenediamine *o*-PD as functional monomers. This biosensor showed a dual-signal oxidation of $\text{Fe}(\text{CN})_6^{4-}$ and PTH-MB at 0.20 V and -0.22 V, respectively. When HSA was captured on MIP, the adsorbed HSA on the electrode surface

would hinder electron transfer, reducing the total intensity of dual-signal currents with the increase of HSA concentration. The limit of detection (LOD) of this sensor can reach $3.0 \times 10^{-11} \text{ g L}^{-1}$. Moreover, the selected AuNPs and PTH-MB both have excellent electrocatalytic performance, in which the methylene blue (MB) in PTH-MB molecules acts as an electrocatalyst, which can enhance the electron transfer efficiency of electrochemical reactions on the electrode surface. Furthermore, the synergistic effect between AuNPs and PTH-MB effectively enhances the current signal, thus improving the sensitivity of the biosensor [21]. In practical detection, this biosensor has good selectivity and repeatability, achieving the detection of HSA in urine, and providing a potential universal platform for clinical protein detection.

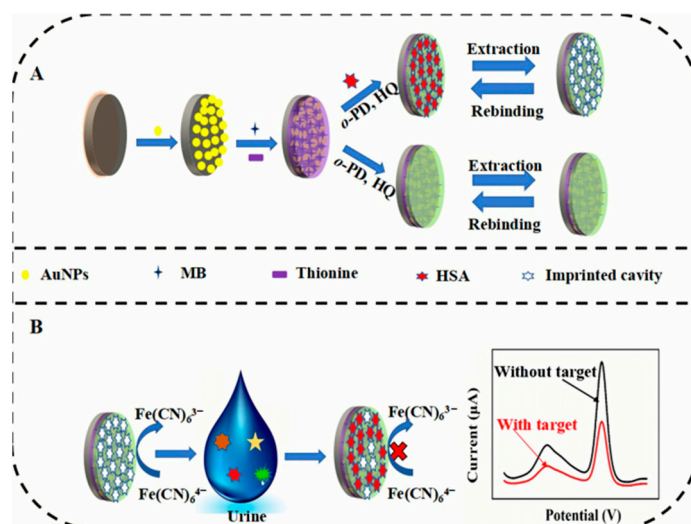


Figure 1. (A) Schematic of the proposed procedure for constructing the molecularly imprinted polymer electrochemical biosensor. (B) Principle of MIP-ECS detection of HSA [20].

2.2. Creatinine (Crn)

Crn is formed in everyday muscle wear and tear and is an important biomarker of renal qualitative and quantitative function. Crn levels play an important role in calculating muscle and renal function. The normal range of urinary Crn is about 282–2600 ppm. The normal range of serum Crn for women is 0.5–1.1 mg/dL (5–11 ppm) and for men is 0.6–1.2 mg/dL (6–12 ppm). Concentrations above 15 ppm require medical attention, and above 59 ppm indicate serious kidney damage [22]. The kidneys filter plasma through the processes of glomerular filtration and tubular excretion, thereby removing Crn to maintain homeostasis in the body. Crn content is helpful in quantifying the GFR, which is a very important indicator of kidney function and has been proven to be a potential biomarker for DN [23]. Clinically, early detection of renal impairment and the implementation of appropriate treatment measures can slow the progression of diabetic nephropathy by monitoring the levels of the albumin-to-Crn ratio [24].

Prabhu et al. [25] developed an instant medical (Point-of-Care, PoC) sensor device based on LoRaWAN (Long Range Wide Area Network, remote wide area network). In this strategy, Crn was used as the template, methacrylic acid (MAA) as the functional monomer, 2,2-azoisobutronitrile (AIBN) as the reaction initiator, and divinylbenzene (DVB) as the cross-linking agent. MIP prepared by standard chemical methods using precipitation polymerization effectively coated the sensor surface with MIP by acrylic resin, making the sensing interface highly functionalized. The constructed sensor has a high specificity for selective adsorption of Crn molecules, and the electrochemical impedance spectrum (EIS) can accurately detect different levels of Crn content. The detection limit is as low as 0.1 ppm (Table 1). This low-cost, portable device allows patients to self-test at home, and the results obtained from this system can help doctors take necessary measures, which is

conducive to early detection and treatment of kidney injury to avoid further deterioration of diabetic nephropathy.

In recent years, the advantages of N-MIT compared with traditional MIP preparation methods have attracted widespread attention. Currently, the common technique for preparing N-MIPs is solid-phase synthesis. In traditional methods for preparing MIPs, the TM are dispersed in the liquid medium, while the solid-phase synthesis method anchors the TM on a specific solid support, and subsequently carries out affinity purification of N-MIPs [26]. Raquel et al. synthesized N-MIPs with advantages such as high affinity, high specificity, excellent stability, and immobilized templates by uniformly distributing imprint nanoparticles in a polyvinyl chloride membrane through precipitation polymerization [27]. In particular, N-MIPs have a large specific surface area, which can expose more binding sites for recognizing small molecules or large biological molecules such as proteins, promoting the development of the imprinting material towards broader application prospects. On the other hand, electrochemiluminescence (ECL) has unique characteristics that differ from other electrochemical methods, such as high signal-to-noise ratio, high sensitivity, wide linear range, high temporal and spatial resolution, and near-zero background light [28]. Developing new chemiluminescence systems is one of the important ways to expand the detection range of ECL [29,30]. Babamiri et al. [31] synthesized nickel nanoclusters (NiNCs) as a new luminescent body and constructed an MIECS based on ECL for Crn detection. A molecularly imprinted polymer (MIP) @ GO-Fe₃O₄ film was constructed on the surface of an indium tin oxide (ITO) electrode using Crn as the template, tetraethyl orthosilicate (TEOS) as the cross-linking agent, and magnetic graphene oxide (GO-Fe₃O₄) as the modifier and embedded nickel nanoclusters (NiNCs). Due to the excellent conductivity of GO-Fe₃O₄, the MIECS retained the high specificity of the MIP @ GO-Fe₃O₄ template for Crn, while significantly improving its sensitivity. In addition, NiNCs have strong and stable ECL with co-reactant TPA, whereas Crn has a quenching effect on NiNCs' ECL, causing the ECL signal intensity to decrease as Crn concentration increases. The detection limit for Crn in serum and urine samples is 0.5 nmol/L (Table 1).

Traditional imprinting methods prepare MIPs that embed most of the binding sites and nanoscale sensitizing materials, making it difficult for TM to wash off from the highly cross-linked heterogeneous rigid polymer structure, and at the same time, obstructing the electronic transport of nanoscale sensitizing materials, which leads to poor sensitivity of ECS. Qian et al. immobilized bovine serum albumin (BSA) templates on the surface of SiO₂ nanoparticles and synthesized surface-modified MIPs [32]. The results showed that surface MIT can reduce the "embedding" phenomenon, and the MIPs prepared by controlling the template location on the material surface or near the surface have high specificity, high affinity, good reproducibility, as well as advantages such as high imprinting efficiency, high binding capacity, and fast speed, providing a good analytical and detection platform for the imprinting of large molecules such as proteins, cells, and viruses. Li et al. [33] reported a novel graphene nanoplatelet (GNP)/polydopamine (PDA)-MIP-biosensor for ultra-trace detection of Crn in a range of body fluids (Figure 2). Under the catalytic action of ammonium persulfate (AP), dopamine hydrochloride (DA) monomer was polymerized on the surface of GNP forming a thin PDA-MIP layer with high-density Crn recognition sites. This novel surface MIP technology avoids overly thick MIP layers, thereby allowing more TM to anchor on or near the polymer surface during the polymerization process. This ensures that the TM can be more thoroughly removed, leading to a broader detection range (Table 1).

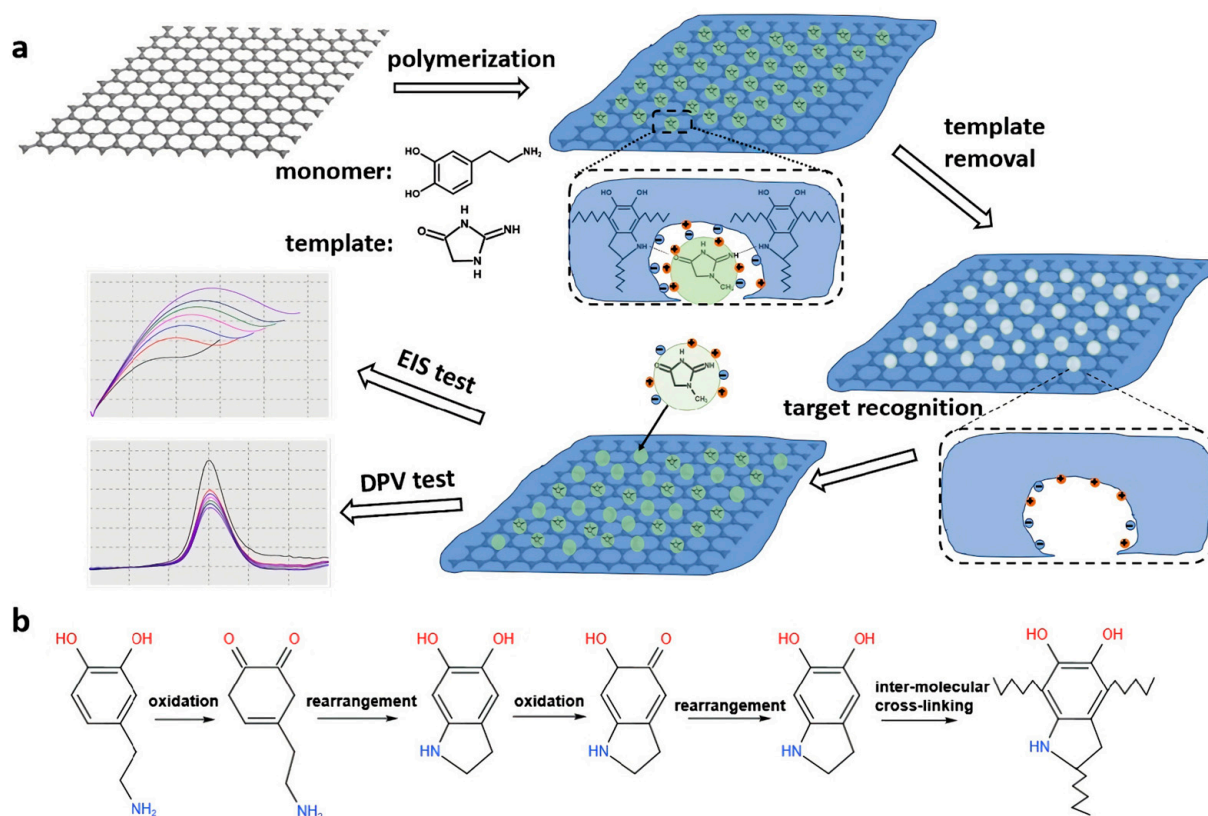


Figure 2. Schematic representation for the preparation of GNP/PDA-MIP. (a) The fabrication and application process of GNP/PDA-MIP and the EIS/DPV response of the GNP/PDA-MIP modified electrode towards different concentration of creatinine in electrolyte. (b) The formation mechanism of DA spontaneous oxidative polymerization [33].

Table 1. The developed BRBS for the detection of Crn.

Category of Technology	Functional Monomer	Detection Limit	Ref.
Traditional-MIT	methacrylic acid	0.1 ppm	[25]
N-MIT	nickel nanoclusters	0.5 nmol/L	[31]
Surface MIT	dopamine hydrochloride	2×10^{-2} pg/mL	[33]

2.3. Cystatin C (Cys-C)

Cys-C is a 13 kDa non-glycosylated polypeptide chain consisting of 120 amino acid residues. It is a small protein that can be freely filtered by the renal glomerulus. The average serum Cys-C level in patients with diabetic nephropathy (1.87 ± 0.51 mg/L) is higher than that in patients with non-diabetic nephropathy (1.025 ± 0.30 mg/L). In addition, serum Cys-C levels are higher in patients with elevated serum Crn levels, suggesting a correlation between Cys-C and Crn. Studies have shown that serum Cys-C detection can help to identify early renal impairment in diabetic patients, with better efficacy than serum Crn [34]. Another study showed that the average serum cystatin C value was 1.73 in type 2 diabetic patients with normal urinary albumin levels, while the average serum cystatin C value was 2.07 in type 2 diabetic patients with microalbuminuria. These results suggest that serum cystatin C, as a renal glomerular filtration biomarker, is an earlier indicator of diabetic nephropathy than urinary microalbumin and serum Crn [35].

Multifunctional monomer imprinting can enhance non-covalent binding between functional monomers and TM via multiple synergistic interaction sites [36]. This is particularly effective in improving the selectivity and adsorption of MIPs for large molecules. Therefore, it is an effective technique to use two or more functional monomers simultaneously,

forming multiple complementary interaction sites with TM in different areas. However, the selection, combination, design, synthesis, and full utilization of their synergistic effect to prepare ideal MIPs still require continuous exploration. In addition, polypyrrole (PPy) is a conductive polymer that is well-known for its use in MIP materials [37]. Carbon nanotubes (CNTs) can improve electron transfer and surface area in electrochemical systems, thereby enhancing the electrical properties of electrochemical biosensors. Therefore, after adding CNTs to PPy, a 3D structure with increased electrical conductivity is formed due to the strong π - π bonding between the Ppy-conjugated structure and CNTs [38]. The PPy/CNT nanocomposite exhibits good charge transfer and energy/electron storage performance, making it suitable for supercapacitors [39]. Based on this strategy, Gomes [40] et al. first formed a mixed system of Cys-C, multi-walled carbon nanotubes (MWCNTs), pyrrole (Py), and carboxylated pyrrole (Py-COOH), and electrochemically polymerized it on the surface of a carbon fiber net screen-printed electrode (SPE) to form an MPPy nanocomposite. Subsequently, the Cys-C template was removed by the urea method, constructing a disposable biosensor based on molecular imprinting capable of accurately detecting Cys-C. Because Cys-C has a higher affinity with binding sites when surrounded by bifunctional monomers, the recognition ability of the sensor is enhanced. Additionally, introducing MWCNTs into the PPy matrix resulted in a more porous structure, larger surface area, and better sensitivity. The differential pulse voltammetry (DPV) detection of Cys-C in a pH 6.0 solution containing $\text{Fe}(\text{CN})_6^{3-/4-}$ using this sensor had a limit of detection (LOD) as low as 0.5 ng/mL, demonstrating its cost-effectiveness and high stability for potential applications in clinical medicine.

2.4. Homocysteine (Hcy)

Hcy, cysteine (Cys), and glutathione (GSH) are the three most abundant small-molecule amino acids containing thiol groups, playing important roles in biological processes [41]. The normal level of Cys in human blood plasma is 135.8–266.5 $\mu\text{mol/L}$, the concentration of Hcy is in the range of 5–15 $\mu\text{mol L}^{-1}$, and the GSH concentration in most cells is at mmol/L level [42,43]. Among them, Hcy is one of the important biomarkers of diabetic nephropathy. Therefore, it is particularly important to establish sensitive, accurate, and highly selective Hcy sensors.

Currently, electrochemical sensors (ECS) are commonly modified with noble metal nanoparticles on their surfaces. For example, Au nanoparticles (AuNPs) [44] possess good electron density, dielectric performance, and catalytic activity, as well as excellent conductivity, stability, and surface adsorption [45]. In recent years, silver nanoparticles [46] and alloy particles [47,48] have also been widely employed in ECS. In addition, MXene, with a chemical formula generally represented as $\text{M}_{n+1}\text{X}_n\text{T}_x$ [49], is an emerging class of two-dimensional inorganic composite materials. MXene demonstrates immense advantages in areas such as medicine and sensing due to its large surface area, excellent energy storage performance, good bioconductivity, and biocompatibility [50,51]. Moreover, MXene possesses a strong reducing ability, providing new strategies for synthesizing multifunctional nano-hybrids [52,53]. Its exceptional performance offers new possibilities for improving the conductivity, electrocatalytic activity, and sensitivity of the target analyte's signal response in biomimetic recognition bio-ECS interfaces. Liu [54] and others developed an unmarked molecularly imprinted electrochemical sensor (MIECS) for rapid and highly sensitive detection of Hcy. In this strategy, AuNPs were first prepared using chloroauric acid as a raw material in the presence of a reducing agent, and then AuNPs were introduced into the multilayer nanostructure of MXene to form MXene@AuNPs nanocomposites. Finally, the MIP with Hcy-specific recognition was formed by electropolymerization of DA monomer on the MXene@AuNPs-modified GCE surface. The MXene in the sensing interface has strong reducibility and excellent conductivity, and its large surface area accommodates more AuNPs and active sites, significantly enhancing the electrochemical performance of the sensor. The Hcy in the sample was detected by cyclic voltammetry, and the current signal decreased with the increase of Hcy concentration, with an LOD of 11.81 fmol L^{-1}

(Table 2). It is worth noting that due to the inherent two-dimensional structure of MXene with stack ability, the target molecules cannot approach the active region [55], which greatly reduces the sensitivity of detecting target molecules, greatly limiting its electrochemical performance. Therefore, the improvement of MXene function and performance is still the focus of current researchers.

Wen [56] and others prepared an Aptasensor using a graphene sponge (GS) as a material (Figure 3). The GS and AuNPs were separately modified on the glassy carbon electrode (GCE). Then, an Hcy APT with 66 bases of hairpin deoxyribonucleic acid (DNA) was fixed on the GCE by a Au-S covalent bond. Non-linking sites were blocked by bovine serum albumin (BSA) using mechanical filling and adsorption coverage methods. Finally, MB was specifically adsorbed on the APT due to its high affinity with guanine [57,58]. In this study, MB had good biocompatibility and could generate electrochemical signals at a specific voltage in DPV, acting as an electrochemical hybridization indicator. In the presence of Hcy, the conformation of the nucleic acid APT changed after specifically binding with Hcy, causing MB release from the APT or moving away from the GCE surface, and thus changing the relative redox current (ΔI) of MB. The sensor exhibited excellent signal detection, selectivity, and reproducibility, with a good linear relationship between Hcy concentration and ΔI in the linear range of 1~100 μM , a wide linear range, and a detection limit of 1 μM (Table 2).

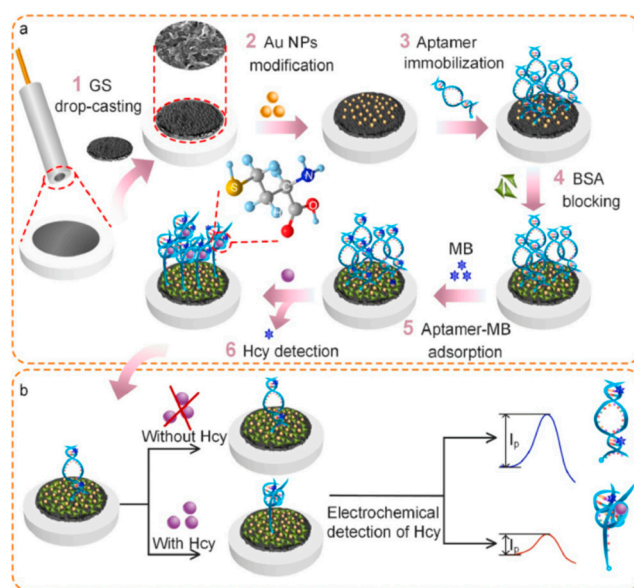


Figure 3. The fabrication procedures and detection mechanism of the aptasensor. (a) The stepwise modifications of the GCE surface. (b) The electrochemical response of the aptasensor with/without Hcy. I_p represents the peak current [56].

APT can effectively recognize biomarkers by non-specifically adsorbing on the surface of gold electrodes or AuNPs. Small molecule-assisted technology (SMAT) refers to the formation of an auxiliary interface by small molecules that enable the linear chains of APT to be vertically oriented on the interface. The specificity of APT is enhanced by restricting the non-specific binding sites at the sensor interface through 6-mercaptohexanol, dithiothreitol, and 3-mercaptopropionic acid. Existing research reports that the binary self-assembled monolayer composed of thiol APT and 6-mercaptohexanol can significantly reduce the surface molecular density of APT, confirming that SMAT can reduce the non-specific adsorption of APT [59]. Hcy is a type of redox molecule [60]. Using SMAT Beitollahi et al. [61] developed an unlabeled electrochemical sensor for detecting Hcy (Figure 4). Firstly, the aptamer solution was cast onto the surface of a glassy carbon electrode modified with AuNPs, and stood upright in a humid room to complete the self-assembly of the thiol aptamer. The modified glassy carbon electrode was then immersed in a 6-mercaptohexanol

solution and washed with 0.1 M PBS at a pH of 7.4. Small molecule interface technology was used to form a linearly coordinated aptamer chain and limit non-specific binding sites. The Hcy binds through interaction with the aptamer and undergoes an electrochemical reaction at the modified electrode surface, resulting in a significant enhancement of the peak current. This sensor, under optimal conditions, identifies Hcy using the differential pulse voltammetry (DPV) method. The detection limit is 0.01 μM , and the linear range is 0.05–20.0 μM (Table 2).

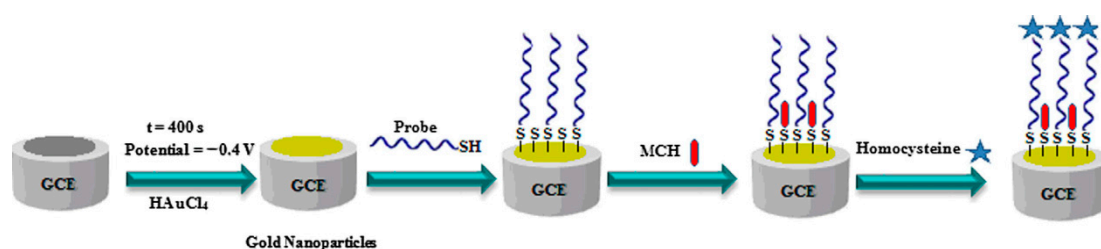


Figure 4. Schematic illustration of stepwise homocysteine aptasensor fabrication process [61].

Table 2. The developed BRBS for the detection of Hcy.

Category of Technology	Functional Monomer/APT	Detection Limit	Ref.
N-MIT	dopamine hydrochloride	11.81 fmol L^{-1}	[54]
MAMT	APT	1 μM	[56]
SMAT	APT	0.01 μM	[61]

2.5. Vascular Endothelial Growth Factor (VEGF)

VEGF is a 45 kDa homodimeric glycoprotein encoded by a single gene. Currently, five human VEGF microRNAs (mRNAs) have been found by splicing of VEGF mRNA, encoding VEGF with 121, 145, 165, 189, and 206 amino acids, respectively [62,63]. It has been found that the glomerular basement membrane has a high affinity for VEGF, which can cause an increase in the permeability of the glomerular basement membrane, thereby promoting the production of NO, endothelin, etc., further changing the renal hemodynamics of diabetic patients, leading to proteinuria and inducing diabetic nephropathy [64]. Therefore, the development of highly sensitive and selective VEGF detection methods is of great significance for early diagnosis and patient recovery assessment.

Palabiyik [65] and others proposed a highly sensitive label-free impedance sensor based on molecularly imprinted polymers (MIP) and graphite screen-printed electrodes (GSPE) as a detection platform for vascular endothelial growth factor (VEGF) (Figure 5). To improve the reproducibility of electrode detection and remove any impurities generated during the electrode manufacturing process, the GSPE was electrochemically pretreated before use. Then, MIP was formed on the pretreated GSPE surface by electropolymerization of ortho-phenylenediamine (o-PD) in the presence of the VGFR template. Under optimized conditions, the sensor used $[\text{Fe}(\text{CN})]^{3-/4-}$ as a redox probe and employed a label-free method based on EIS measurement to detect VGFR, with good analytical performance in the range of 20–200 pg mL^{-1} and a detection limit of 0.08 pg mL^{-1} (Table 3). Due to the disposable nature of the sensor, it is more suitable for clinical needs.

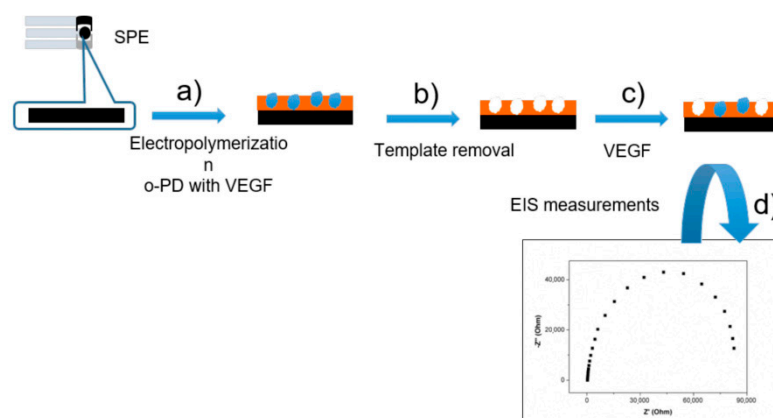


Figure 5. Scheme representation of molecular imprinting and the recognition principle: (a) electropolymerization with o-PD and VEGF; (b) removal of VEGF template; (c) incubation with VEGF sample solution; (d) washing and EIS measurements [65].

Cheng [66] and others constructed a convenient and ultra-sensitive ECL APT biosensor for detecting VEGF165. Firstly, the synthesized graphite-like carbon nitride (g-C₃N₄) nanosheets were adhered to CdSe using polydiallyldimethylammonium chloride (PDDA) as an adhesive, followed by assembling the obtained g-C₃N₄/PDDA/CdSe composite material onto the GCE surface. Finally, DNA₁ and AuNP-labeled DNA₂ were sequentially incubated on the modified GCE surface. In this strategy, AuDNA₂ showed a significant spectral overlap with the g-C₃N₄/PDDA/CdSe composite, thus allowing for effective energy transfer. In the presence of VEGF165, the sensor impedance decreased significantly after the Au-DNA₂ binds to VEGF165, and the ECL signal increased significantly. The ECL signal of the constructed biosensor increased with the increasing concentration of VEGF165, showing a prominent linear relationship from 2 pg mL⁻¹ to 2 ng mL⁻¹, and the detection limit of VEGF165 was as low as 0.68 pg mL⁻¹ (Table 3). The excellent sensitivity, stability, repeatability, and selectivity of the ECL biosensor indicate further potential applications in clinical diagnosis.

Table 3. The developed BRBS for the detection of VEGF.

Category of Technology	Functional Monomer/APT	Detection Limit	Ref.
Surface MIT	ortho-phenylenediamine	0.08 pg mL ⁻¹	[65]
MAMT	APT	0.68 pg mL ⁻¹	[66]

2.6. Epidermal Growth Factor Receptor (EGFR)

In recent years, EGFR has been proven to be one of the potential biomarkers for diabetic nephropathy [67]. Generally, the preparation of MIPs typically involves a single kind of template molecule/ion. However, MIPs based on a single template cannot recognize and remove multiple targets simultaneously. Multi-template MIT uses two or more target substances simultaneously as templates. Li et al. achieved simultaneous detection of dopamine and uric acid using dual-template technology, allowing the formation of MIPs containing multiple specific recognition sites. This provides a feasible strategy for simultaneously enriching, recognizing, detecting, and removing multiple targets [68]. Ahar et al. [69] constructed a MIP biosensor based on gold nanoparticle-modified screen-printed electrodes (Au-SPE) and used antibody-coupled nanoliposome amplification for simultaneous detection of EGFR and vascular VEGF (Figure 6). First, DSP was assembled onto the Au-SPE surface by self-assembly, and then the target proteins (EGFR and VEGF) were attached covalently through amide bonds to the modified SPE using multi-template molecular imprinting. Unbound sites were then blocked with acrylamide (AAM). Under the presence of persulfate, the AAM and *N,N'*-methylenebis(acrylamide) functional monomers were

polymerized around the EGFR and VEGF templates, and the polymerization termination time was controlled by mixing the phenol solution with ethanol (w/t, 1%). Finally, by utilizing the ability of oxalic acid (OXA) to destroy peptide bonds, the template molecule is successfully removed from the imprinting layer. This strategy aims to produce reliable electrochemical signals by using nanoliposomes loaded with Cd(II) and Cu(II) ions, and modified with EGFR and VEGF-specific antibodies as the detection targets. In the analysis step, the potentiostatic adsorption electrochemical technique is employed to indirectly determine the trace amounts of EGFR and VEGF in serum based on the content of these ions. Under optimal conditions, the detection limits for EGFR and VEGF analysis are 0.01 and 0.005 pg mL^{-1} , respectively. The sensor has good sensitivity, repeatability, and specificity. In clinical practice, it is often necessary to analyze a series of biomarkers to make a final diagnostic result, and this SPE-based biosensor can be successfully integrated with lab-on-a-chip, microfluidics, or micro-total analytical systems, opening new avenues for the development of multiplexed sensing of biomarkers. However, it is worth noting that due to the dilution of each template's binding sites, the selectivity of multi-template MIPs is lower than MIPs synthesized with a single template.

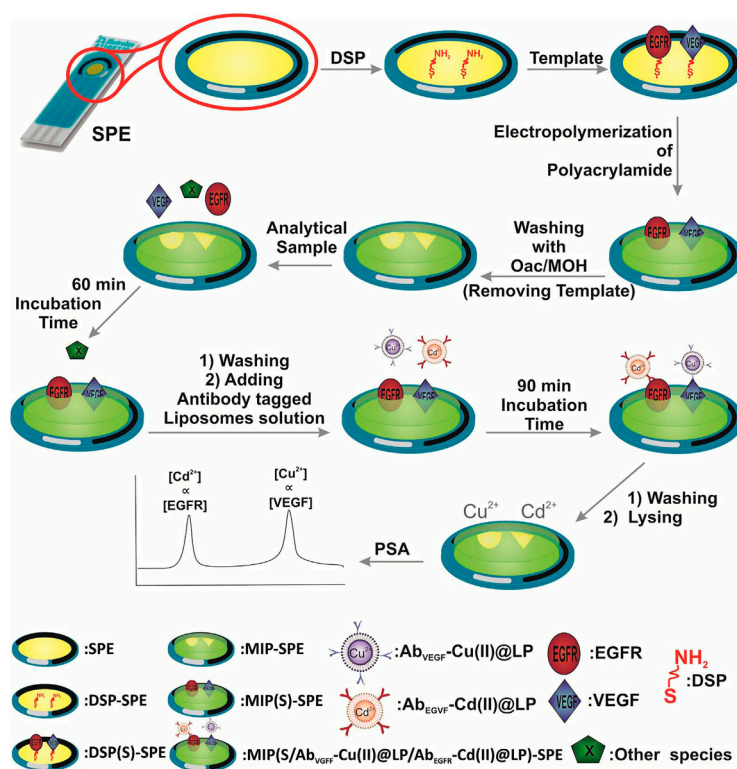


Figure 6. Representation for the engineering processes of EGFR/VEGF biosensors [69].

2.7. mRNA-21

mRNAs are a class of small non-coding RNAs that play important roles in post-transcriptional regulation of gene expression. mRNAs regulate over 60% of protein-coding gene expression. Therefore, changes in their expression are associated with many diseases, including liver diseases, kidney diseases, and diabetes [70–72]. Recently, some of the literature reported that mRNAs, such as mRNA-21, mRNA-223-3p, and mRNA-377, can serve as potential biomarkers for diabetic nephropathy [73,74].

Liu et al. [75] designed a photoelectroactive aptasensor for the detection of mRNA-21. First, chitosan was used to wrap the CuInS_2 -modified ITO electrode surface, preventing the dissolution of CuInS_2 into the solution, and providing amino groups for subsequent electrode modification. Then, the carboxyl-modified DNA₂ reacted with chitosan and was coupled to the electrode via amide bonds. If the hairpin DNA is recognized by

mRNA-21, Exonuclease III (Exo III) will cleave the blunt 3' end of DNA₁, triggering the target-cycled amplification process that releases DNA₃, which can hybridize with DNA₂ on the electrode. The DNA₂–DNA₃ duplex provides a binding site for TATA-binding protein (TBP) attachment. Since TBP induces an 80-degree bend in the TATA sequence by inserting amino acid side chains on the base pairs of the dsDNA sequence [76], this blocks electron transfer, causing a sharp decrease in photocurrent intensity. The decrease in photocurrent due to steric hindrance can be used to quantify microRNA-21. This strategy combines anti-interference photoelectroactive cathode materials, enzyme-assisted target cycle amplification, and TBP-induced signal shutdown, achieving remarkable amplification efficiency. The detection limit of mRNA-21, under optimized conditions, is as low as 0.47 fM, and the linear range is from 1.0×10^{-15} M to 1.0×10^{-9} M. Further research is needed to explore the application of this DNA amplification-based PEC platform in DNA, protein, and small molecule detection.

2.8. Ceruloplasmin (Cp)

Cp is a copper-containing α -2 globulin with a molecular weight of 132 kDa, mainly synthesized and secreted by the liver, and plays a crucial role in regulating oxidative stress and iron homeostasis [77]. Some researchers have proposed that the glomerular capillary wall excretion rate of Cp in patients with diabetic nephropathy is almost parallel to the urinary albumin excretion rate. Increased excretion of Cp has also been observed in patients with impaired glucose tolerance and diabetes compared to healthy controls [78]. Increased urinary Cp excretion in diabetic patients with normal urinary protein has also been confirmed [79]. Therefore, detecting urinary Cp has a high value for early diagnosis of diabetic nephropathy.

Haghshenas et al. [80] designed a sensitive electrochemical aptasensor to quantify Cp using Cp-specific recognition APT. First, the diazonium salt of 4-Aminobenzoic acid (ABA) electrochemically reduced was covalently bonded to the MWCNTs/GCE surface [81], and after the carboxyl group was activated by *N*-hydroxysuccinimide (NHS) and *N*-(3-dimethylaminopropyl)-*N'*-ethylcarbodiimide hydrochloride (EDC), the amino APT was immobilized on the electrode surface via amide bond formation. BSA solution was added to prevent non-specific adsorption on the sensor surface. Finally, Cp was detected using DPV and EIS in $[\text{Fe}(\text{CN})_6]^{3-/4-}$ solution. Cp-specific binding with APT induces a conformational change in the APT on the electrode surface, and the probe's electron transfer is hindered. The DPV current of the aptasensor decreases with increasing Cp concentration, and the Rct value increases with increasing Cp concentration. Under optimal conditions, Cp concentration shows a linear relationship within the range of $0.02\text{--}3.0 \text{ ng mL}^{-1}$ and $3.0\text{--}80.0 \text{ ng mL}^{-1}$, with a detection limit of 3.7 pg mL^{-1} . This aptasensor has broad application prospects for detecting Cp in human serum.

2.9. Platelet-Derived Growth Factor (PDGF)

PDGF is an important cytokine composed of two peptide chains (A and B) connected by disulfide bonds in serum, which can promote the proliferation of vascular endothelial cells, smooth muscle cells, and the biosynthesis of renal tubule matrix, playing a crucial role in regulating cell growth and division [82]. PDGF-AA, PDGF-BB, and PDGF-AB are three subtypes of PDGF [83]. Among them, PDGF-BB is directly involved in cell transformation and tumor growth [84]. Studies have shown that the level of PDGF in the plasma of patients with diabetic nephropathy increases. PDGF can promote the proliferation and matrix generation of renal tubular cells, further accelerating the process of renal fibrosis, which leads to further deterioration of renal function. In addition, PDGF-BB is considered an important marker capable of predicting early deterioration of renal function in patients with diabetic nephropathy. Therefore, the sensitive and selective detection of PDGF-BB in biological samples has significant implications for the diagnosis of diabetic nephropathy.

Zhang et al. [85] introduced an ECL aptasensor based on improved AuNPs to detect PDGF-BB (Figure 7). In this scheme, AuNPs-electrochemically reduced graphene

(AuNPs-EG) nanocomposite material was electrodeposited on the GCE surface, and a large number of PDGF-BB APT (APT_1) were fixed to amplify the detection response, constructing a highly conductive Aptasensor platform that can amplify the Luminol- H_2O_2 system ECL signal. By functionalizing AuNPs with glucose oxidase (GOD), a signal probe for the sandwich sensor of the second aptamer (APT_2) and GOD-modified AuNPs was designed. This ECL sensor has the advantages of high sensitivity, good stability, and good selectivity, and has good analytical performance in the concentration range of $1.0 \times 10^{-13} \sim 5.0 \times 10^{-10} \text{ mol L}^{-1}$ PDGF-BB, with a detection limit of $1.7 \times 10^{-14} \text{ mol L}^{-1}$ (Table 4). It has the potential for application in biochemical analysis.

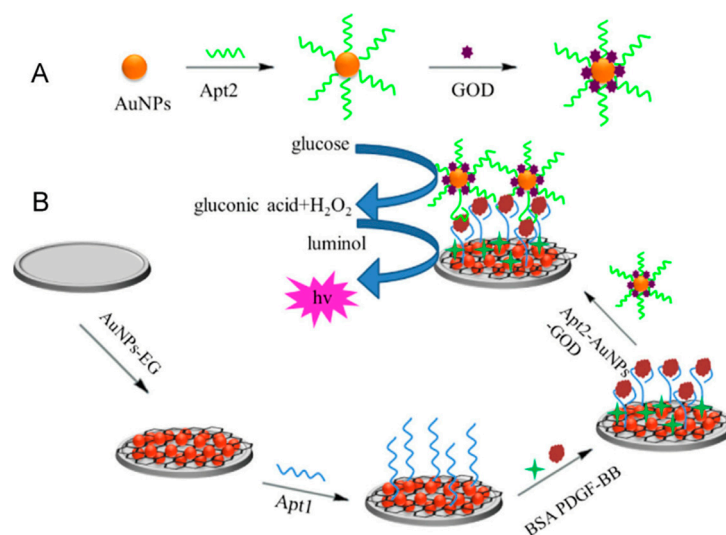


Figure 7. The procedure of the ECL aptasensor preparation. (A) Preparation of GOD-Apt2-AuNPs bioconjugates. (B) The schematic shows the strategy for constructing the ECL aptasensor [85].

In recent years, two-dimensional layered transition metal dichalcogenide materials have opened a new door in the field of electrochemistry due to their unique electronic and electrochemical properties [86]. VS_2 has significant advantages in large specific surface area, good catalytic adsorption performance, and good biocompatibility. Normally, VS_2 has a stacked-layer structure, and the V atom inserts between two S atoms to form a sandwich structure. Unfortunately, like most transition metal oxides, the weak conductivity of VS_2 severely limits its further application in electrochemical biosensors. In order to improve the electrochemical performance of VS_2 , it seems necessary to combine it with good electronic conductive materials. Framework nucleic acids (FNAs) are one-dimensional to three-dimensional (3D) framework structures formed by nucleic acid molecules through self-assembly [87]. The surface performance of electrochemical DNA biosensors modified with FNAs has been significantly improved. Due to the good stability and controllability of FNAs, they can be assembled in an ordered manner on gold surfaces to fabricate more probes [88,89]. The controllable charge transfer characteristics of FNAs can be utilized to optimize the performance of electrochemical biosensors based on FNAs [90]. Compared to traditional electrochemical sensors functionalized with single-stranded DNA, electrochemical biosensors based on FNAs have stronger interference resistance and higher protein resistance. The empty structure allows for the maximization of space utilization, making it highly suitable for interface assembly with various materials [91]. Huang et al. [92] first prepared a novel VS_2 -graphene (VS_2 -GR) composite material using a simple one-step hydrothermal method and a novel label-free electrochemical aptasensor was designed for the detection of platelet-derived growth factor BB (PDGF-BB) using Exo III-assisted signal amplification technology, VS_2 -GR composite material, and tetrahedral structured DNA probe [93,94], which exhibits fast response, high throughput, and current sensitivity. In the absence of PDGE-BB, the APT hybridizes with complementary DNA (cDNA), and

the biotin-labeled single-stranded signal DNA at the 5' end cannot be cleaved by exonuclease III (Exo III). Biotin-labeled signal DNA hybridizes with protruding T-DNA on the AuNP/VS₂-GR electrode, and the specific binding of avidin-biotin absorbs a large amount of avidin-horseradish peroxidase (avidin-HRP) onto the modified electrode, resulting in a strong current response of HRP to the mixture of hydrogen peroxide and hydroquinone (H₂O₂ + HQ). However, when PDGF-BB is present, the APT preferentially binds to PDGF-BB, and duplex DNA is formed between cDNA and signal DNA. The double-stranded DNA is digested by Exo III from the blunt end of the 3' signal DNA and releases cDNA. Subsequently, the released cDNA undergoes a new cleavage process with the remaining signal DNA in the solution. Finally, the cyclic hybridization-hydrolysis process leads to a reduction in the number of signal molecules HRP on the electrode, resulting in a significant decrease in current response. The proposed detection method takes advantage of the large specific surface area, good conductivity, and excellent biocompatibility of layered VS₂-GR composite materials, providing plenty of binding sites and suitable environments for the immobilization of biomolecules. In addition, the tetrahedral structured DNA probe based on framework nucleic acid assembly technology can minimize non-specific adsorption and obtain upright probes on the electrode surface, improving detection stability and reproducibility. Based on these advantages, the proposed detection method can detect PDGF-BB concentrations as low as 30 fM and has good selectivity for PDGF-BB (Table 4). Due to the inherent characteristics of Exo III, which does not require specific recognition sites and APT, the proposed detection method has a wide range of target molecules and can serve as a universal scheme for detecting DNA, drugs, and even proteins.

Table 4. The developed BRBS for the detection of PDGF.

Category of Technology	Functional Monomer/APT	Detection Limit	Ref.
MAMT	APT	1.7×10^{-14} mol L ⁻¹	[85]
FNAs	APT	30 fM	[92]

3. Conclusions and Future Perspectives

Significant progress has been made in the construction technology of biomimetic recognition electrochemical sensors for diabetic nephropathy biomarkers, but there are still many challenges at the current stage. Current challenges include developing new multifunctional recognition elements, simultaneous detection of multiple biomarkers, further studying the binding mechanism between MIPs and target objects, achieving specific recognition of MIPs in the aqueous phase, enhancing the effective recognition rate of recognition elements for large molecules and the anti-interference ability of complex samples, integrating recognition elements and transducers to increase the sensitivity of sensors, making their preparation more convenient and faster, and further promoting their development towards intelligence and portability. With the rapid development of biotechnology, intelligent control technology, and microelectronics technology, especially micro-electro-mechanical systems (MEMS), the future biomimetic sensors will be miniaturized intelligent biomimetic systems supported by continuous system integration technology. Currently, it seems that miniaturized intelligent biomimetic sensors may be one of the main choices for the future construction of the perception layer sensors in the Internet of Things, and could be the only possible choice to replace traditional sensors.

Funding: This project was kindly funded by the National Natural Science Foundation of China (Nos. 22174136, 22004116), and the CAS President's International Fellowship Initiative (PIFI) (No. 2023VBC0020).

Institutional Review Board Statement: Not applicable.

Informed Consent Statement: Not applicable.

Conflicts of Interest: The authors declare no conflict of interest.

References

1. Fawzy, M.S.; Al Beladi, F.I. Association of Circulating Vitamin D, VDBP, and Vitamin D Receptor Expression with Severity of Diabetic Nephropathy in a Group of Saudi Type 2 Diabetes Mellitus Patients. *Clin. Lab.* **2018**, *64*, 1623–1633. [[CrossRef](#)] [[PubMed](#)]
2. Hayes, A.; Arima, H.; Woodward, M.; Chalmers, J.; Poulter, N.; Hamet, P.; Clarke, P. Changes in Quality of Life Associated with Complications of Diabetes: Results from the ADVANCE Study. *Value Health* **2016**, *19*, 36–41. [[CrossRef](#)] [[PubMed](#)]
3. Thorn, L.M.; Gordin, D.; Harjutsalo, V.; Hagg, S.; Masar, R.; Saraheimo, M.; Tolonen, N.; Waden, J.; Groop, P.H.; Forsblom, C.M.; et al. The Presence and Consequence of Nonalbuminuric Chronic Kidney Disease in Patients With Type 1 Diabetes. *Diabetes Care* **2015**, *38*, 2128–2133. [[CrossRef](#)] [[PubMed](#)]
4. Du, Y.; Xu, B.J.; Deng, X.; Wu, X.W.; Li, Y.J.; Wang, S.R.; Wang, Y.N.; Ji, S.; Guo, M.Z.; Yang, D.Z.; et al. Predictive metabolic signatures for the occurrence and development of diabetic nephropathy and the intervention of Ginkgo biloba leaves extract based on gas or liquid chromatography with mass spectrometry. *J. Pharm. Biomed. Anal.* **2019**, *166*, 30–39. [[CrossRef](#)]
5. Chen, Y.; Liu, H.; Loh, T.P.; Liu, Q.; Teo, T.L.; Lee, T.K.; Sethi, S.K. Measurement of urine albumin by liquid chromatography-isotope dilution tandem mass spectrometry and its application to value assignment of external quality assessment samples and certification of reference materials. *Clin. Chem. Lab. Med.* **2021**, *59*, 711–720. [[CrossRef](#)]
6. Ji, H.; Shen, L.; Shi, X.; Su, J.; Tang, Z.; Wang, H.; Ju, S.; Wang, J. Establishment of an absolute quantitative method for measurement of urinary cystatin C by stable isotope dilution ultra high performance liquid chromatography tandem mass spectrometry. *Anal. Methods* **2018**, *10*, 5236–5241. [[CrossRef](#)]
7. Harlan, R.; Clarke, W.; Di Bussolo, J.M.; Kozak, M.; Straseski, J.; Meany, D.L. An automated turbulent flow liquid chromatography-isotope dilution mass spectrometry (LC-IDMS) method for quantitation of serum creatinine. *Clin. Chim. Acta.* **2010**, *411*, 1728–1734. [[CrossRef](#)]
8. Wang, H.; Chai, Y.; Li, H.; Yuan, R. Sensitive electrochemiluminescent immunosensor for diabetic nephropathy analysis based on tris(bipyridine) ruthenium(II) derivative with binary intramolecular self-catalyzed property. *Biosens. Bioelectron.* **2018**, *100*, 35–40. [[CrossRef](#)]
9. Li, Y.; Wang, Y.; Bai, L.; Lv, H.; Huang, W.; Liu, S.; Ding, S.; Zhao, M. Ultrasensitive electrochemiluminescent immunosensing based on trimetallic Au-Pd-Pt/MoS(2) nanosheet as coreaction accelerator and self-enhanced ABEI-centric complex. *Anal. Chim. Acta.* **2020**, *1125*, 86–93. [[CrossRef](#)]
10. Xu, H.; Kou, F.; Ye, H.; Wang, Z.; Huang, S.; Liu, X.; Zhu, X.; Lin, Z.; Chen, G. Highly sensitive antibody-aptamer sensor for vascular endothelial growth factor based on hybridization chain reaction and pH meter/indicator. *Talanta* **2017**, *175*, 177–182. [[CrossRef](#)]
11. Wang, H.; Ma, Y.; Guo, C.; Yang, Y.; Peng, Z.; Liu, Z.; Zhang, Z. Templated seed-mediated derived Au nanoarchitectures embedded with nanochitosan: Sensitive electrochemical aptasensor for vascular endothelial growth factor and living MCF-7 cell detection. *Appl. Surf. Sci.* **2019**, *481*, 505–514. [[CrossRef](#)]
12. Hassanzadeh, M.; Ghaemy, M.; Amininasab, S.M.; Shami, Z. Molecularly imprinted polymer capped near infrared fluorescent emitting Ag₂S-functionalized-COOH quantum dots for detection of creatinine as a nanosensor with high sensitivity and selectivity. *Sens. Actuators A Phys.* **2021**, *331*, 112936. [[CrossRef](#)]
13. Zhuang-Fei, J.; Qin, L.; Qing-Yao, L.; Hui-Xian, X.; Jia-Yuan, H.; Chong-Zhi, W.; Lian-Di, Z.; Qi-Hui, Z.; Ling, L.; Chun-Su, Y. Fast exhaustive enrichment and electrochemical quantitative detection of anthocyanins from natural products by using dual responsive and dummy molecularly imprinted polymers. *Microchem. J.* **2022**, *179*, 107545.
14. Taghdisi, S.M.; Danesh, N.M.; Ramezani, M.; Alibolandi, M.; Nameghi, M.A.; Gerayelou, G.; Abnous, K. A novel electrochemical aptasensor for ochratoxin a sensing in spiked food using strand-displacement polymerase reaction. *Talanta* **2021**, *223 Pt 1*, 121705. [[CrossRef](#)] [[PubMed](#)]
15. Yan, S.R.; Foroughi, M.M.; Safaei, M.; Jahani, S.; Ebrahimpour, N.; Borhani, F.; Rezaei Zade Baravati, N.; Aramesh-Boroujeni, Z.; Foong, L.K. A review: Recent advances in ultrasensitive and highly specific recognition aptasensors with various detection strategies. *Int. J. Biol. Macromol.* **2020**, *155*, 184–207. [[CrossRef](#)]
16. Kimura-Suda, H.; Petrovykh, D.Y.; Tarlov, M.J.; Whitman, L.J. Base-dependent competitive adsorption of single-stranded DNA on gold. *J. Am. Chem. Soc.* **2003**, *125*, 9014–9015. [[CrossRef](#)] [[PubMed](#)]
17. Wang, S.; Cai, X.; Wang, L.; Li, J.; Li, Q.; Zuo, X.; Shi, J.; Huang, Q.; Fan, C. DNA orientation-specific adhesion and patterning of living mammalian cells on self-assembled DNA monolayers. *Chem. Sci.* **2016**, *7*, 2722–2727. [[CrossRef](#)]
18. McTaggart, M.P.; Price, C.P.; Pinnock, R.G.; Stevens, P.E.; Newall, R.G.; Lamb, E.J. The Diagnostic Accuracy of a Urine Albumin-Creatinine Ratio Point-of-Care Test for Detection of Albuminuria in Primary Care. *Am. J. Kidney Dis.* **2012**, *60*, 787–794. [[CrossRef](#)]
19. MacIsaac, R.J.; Ekinci, E.I.; Jerums, G. Markers of and Risk Factors for the Development and Progression of Diabetic Kidney Disease. *Am. J. Kidney Dis.* **2014**, *63*, S39–S62. [[CrossRef](#)]
20. Zhang, G.; Yu, Y.; Guo, M.; Lin, B.; Zhang, L. A sensitive determination of albumin in urine by molecularly imprinted electrochemical biosensor based on dual-signal strategy. *Sens. Actuators B Chem.* **2019**, *288*, 564–570. [[CrossRef](#)]
21. Boon, E.M.; Ceres, D.M.; Drummond, T.G.; Hill, M.G.; Barton, J.K. Mutation detection by electrocatalysis at DNA-modified electrodes. *Nat. Biotechnol.* **2000**, *18*, 1096–1102. [[CrossRef](#)]
22. Kintzel, P.E. Anticancer drug-induced kidney disorders. *Drug Saf.* **2001**, *24*, 19–38. [[CrossRef](#)]
23. Levey, A.S.; Perrone, R.D.; Madias, N.E. Serum Creatinine and Renal Function. *Annu. Rev. Med.* **1988**, *39*, 465–490. [[CrossRef](#)]

24. Musa, N.; Ramzy, T.; Hamdy, A.; Arafa, N.; Hassan, M. Assessment of urinary podocalyxin as a marker of glomerular injury in obesity-related kidney disease in children and adolescents with obesity compared to urinary albumin creatinine ratio. *Clin. Obes.* **2021**, *11*, e12452. [[CrossRef](#)] [[PubMed](#)]
25. Prabhu, S.N.; Mukhopadhyay, S.C.; Gooneratne, C.P.; Davidson, A.S.; Liu, G. Molecularly Imprinted Polymer-based detection of creatinine towards smart sensing. *Med. Devices Sens.* **2020**, *3*, e10133. [[CrossRef](#)]
26. Canfarotta, F.; Poma, A.; Guerreiro, A.; Piletsky, S. Solid-phase synthesis of molecularly imprinted nanoparticles. *Nat. Protoc.* **2016**, *11*, 443–455. [[CrossRef](#)]
27. Gutiérrez-Climente, R.; Gómez-Caballero, A.; Unceta, N.; Aránzazu Goicolea, M.; Barrio, R.J. A new potentiometric sensor based on chiral imprinted nanoparticles for the discrimination of the enantiomers of the antidepressant citalopram. *Electrochim. Acta* **2016**, *196*, 496–504. [[CrossRef](#)]
28. Meng, C.; Knežević, S.; Du, F.; Guan, Y.; Kanoufi, F.; Sojic, N.; Xu, G. Recent advances in electrochemiluminescence imaging analysis. *eScience* **2022**, *2*, 591–605. [[CrossRef](#)]
29. Quan, S.; Ji, K.; Liu, F.; Barkae, T.H.; Halawa, M.I.; Hanif, S.; Lou, B.; Li, J.; Xu, G. Chemiluminescence of lucigenin-tetracycline and its application for sensitive determination of procyanidin. *J. Food Drug Anal.* **2022**, *30*, 293–302. [[CrossRef](#)]
30. Mostafa, I.M.; Gilani, M.; Chen, Y.; Lou, B.; Li, J.; Xu, G. Lucigenin-pyrogallol chemiluminescence for the multiple detection of pyrogallol, cobalt ion, and tyrosinase. *J. Food Drug Anal.* **2021**, *29*, 510–520. [[CrossRef](#)]
31. Babamiri, B.; Salimi, A.; Hallaj, R.; Hasanzadeh, M. Nickel nanoclusters as a novel emitter for molecularly imprinted electrochemiluminescence based sensor toward nanomolar detection of creatinine. *Biosens. Bioelectron.* **2018**, *107*, 272–279. [[CrossRef](#)] [[PubMed](#)]
32. Chen, L.; Wang, X.; Lu, W.; Wu, X.; Li, J. Molecular imprinting: Perspectives and applications. *Chem. Soc. Rev.* **2016**, *45*, 2137–2211. [[CrossRef](#)]
33. Li, Y.; Luo, L.; Nie, M.; Davenport, A.; Li, Y.; Li, B.; Choy, K.L. A graphene nanoplatelet-polydopamine molecularly imprinted biosensor for Ultratrace creatinine detection. *Biosens. Bioelectron.* **2022**, *216*, 114638. [[CrossRef](#)]
34. Amer, A.H.; Haridas, N. Early Diagnostic Markers in Diabetic Nephropathy Patients. *J. Clin. Diagn. Res.* **2018**, *12*, BC05–BC09. [[CrossRef](#)]
35. Gupta, K.; Nayyar, S.B.; Sachdeva, J.K.; Kumar, P. Cystatin C in the early diagnosis of diabetic nephropathy and its correlation with albuminuria. *Int. J. Adv. Med.* **2017**, *4*, 56–59. [[CrossRef](#)]
36. Dingding, D.; Jun, W.; Pengxin, H.; Xin, L.; Luhang, Z.; Shenao, M. Dual-monomer molecularly imprinted electrochemical sensor based on amino-functionalized MOFs and graphene for trace determination of taurine. *Mikrochim. Acta* **2023**, *190*, 126–162.
37. Hoefer, M.; Bandaru, P.R. Determination and enhancement of the capacitance contributions in carbon nanotube based electrode systems. *Appl. Phys. Lett.* **2009**, *95*, 183108. [[CrossRef](#)]
38. Ferreira, P.A.B.; Araujo, M.C.M.; Prado, C.M.; de Lima, R.A.; Rodriguez, B.A.G.; Dutra, R.F. An ultrasensitive Cystatin C renal failure immunosensor based on a PPy/CNT electrochemical capacitor grafted on interdigitated electrode. *Colloids Surf. B Biointerfaces* **2020**, *189*, 110834. [[CrossRef](#)]
39. Canobre, S.C.; Xavier FF, S.; Fagundes, W.S.; de Freitas, A.C.; Amaral, F.A. Performance of the Chemical and Electrochemical Composites of PPy/CNT as Electrodes in Type I Supercapacitors. *J. Nanomater.* **2015**, *2015*, 560164. [[CrossRef](#)]
40. Gomes, R.S.; Gomez-Rodriguez, B.A.; Fernandes, R.; Sales, M.G.F.; Moreira, F.T.C.; Dutra, R.F. Plastic Antibody of Polypyrrole/Multiwall Carbon Nanotubes on Screen-Printed Electrodes for Cystatin C Detection. *Biosensors* **2021**, *11*, 175. [[CrossRef](#)] [[PubMed](#)]
41. Zhang, B.; Zhang, H.; Zhong, M.; Wang, S.; Xu, Q.; Cho, D.-H.; Qiu, H. A novel off-on fluorescent probe for specific detection and imaging of cysteine in live cells and in vivo. *Chin. Chem. Lett.* **2020**, *31*, 133–135. [[CrossRef](#)]
42. Refsum, H.; Ueland, P.M.; Nygard, O.; Vollset, S.E. Homocysteine and Cardiovascular Disease. *Annu. Rev. Med.* **1998**, *49*, 31–62. [[CrossRef](#)] [[PubMed](#)]
43. Sedgwick, A.C.; Wu, L.; Han, H.H.; Bull, S.D.; He, X.P.; James, T.D.; Sessler, J.L.; Tang, B.Z.; Tian, H.; Yoon, J. Excited-state intramolecular proton-transfer (ESIPT) based fluorescence sensors and imaging agents. *Chem. Soc. Rev.* **2018**, *47*, 8842–8880. [[CrossRef](#)] [[PubMed](#)]
44. Ben Messaoud, N.; Ghica, M.E.; Dridi, C.; Ben Ali, M.; Brett CM, A. Electrochemical sensor based on multiwalled carbon nanotube and gold nanoparticle modified electrode for the sensitive detection of bisphenol A. *Sens. Actuators B Chem.* **2017**, *253*, 513–522. [[CrossRef](#)]
45. Plowman, B.J.; Sidhureddy, B.; Sokolov, S.V.; Young, N.P.; Chen, A.; Compton, R.G. Electrochemical Behavior of Gold-Silver Alloy Nanoparticles. *ChemElectroChem* **2016**, *3*, 1039–1043. [[CrossRef](#)]
46. Kumar, N.; Goyal, R.N. Silver nanoparticles decorated graphene nanoribbon modified pyrolytic graphite sensor for determination of histamine. *Sens. Actuators B Chem.* **2018**, *268*, 383–391. [[CrossRef](#)]
47. Zhou, Y.-C.; Zhao, M.; Yu, Y.-Q.; Lei, Y.-M.; Chai, Y.-Q.; Yuan, R.; Zhuo, Y. Three-dimensional nano-network composed of Pt nanoparticles functionalized Mn-doped CeO₂ and hemin/G-quadruplex as electrocatalysts for cardiovascular biomarker detection. *Sens. Actuators B Chem.* **2017**, *246*, 1–8. [[CrossRef](#)]
48. Yang, L.; Xu, B.; Ye, H.; Zhao, F.; Zeng, B. A novel quercetin electrochemical sensor based on molecularly imprinted poly(para-aminobenzoic acid) on 3D Pd nanoparticles-porous graphene-carbon nanotubes composite. *Sens. Actuators B Chem.* **2017**, *251*, 601–608. [[CrossRef](#)]

49. Xie, Y.; Gao, F.; Tu, X.; Ma, X.; Xu, Q.; Dai, R.; Huang, X.; Yu, Y.; Lu, L. Facile Synthesis of MXene/Electrochemically Reduced Graphene Oxide Composites and Their Application for Electrochemical Sensing of Carbendazim. *J. Electrochem. Soc.* **2019**, *166*, B1673–B1680. [[CrossRef](#)]
50. Wang, H.; Li, H.; Huang, Y.; Xiong, M.; Wang, F.; Li, C. A label-free electrochemical biosensor for highly sensitive detection of gliotoxin based on DNA nanostructure/MXene nanocomplexes. *Biosens. Bioelectron.* **2019**, *142*, 111531. [[CrossRef](#)]
51. Nah, J.S.; Barman, S.C.; Zahed, M.A.; Sharifuzzaman, M.; Yoon, H.; Park, C.; Yoon, S.; Zhang, S.; Park, J.Y. A wearable microfluidics-integrated impedimetric immunosensor based on Ti3C2T MXene incorporated laser-burned graphene for noninvasive sweat cortisol detection. *Sens. Actuators B Chem.* **2021**, *329*, 129206. [[CrossRef](#)]
52. Ma, X.; Tu, X.; Gao, F.; Xie, Y.; Huang, X.; Fernandez, C.; Qu, F.; Liu, G.; Lu, L.; Yu, Y. Hierarchical porous MXene/amino carbon nanotubes-based molecular imprinting sensor for highly sensitive and selective sensing of fisetin. *Sens. Actuators B Chem.* **2020**, *309*, 127815. [[CrossRef](#)]
53. Mohammadniaei, M.; Koyappayil, A.; Sun, Y.; Min, J.; Lee, M.H. Gold nanoparticle/MXene for multiple and sensitive detection of oncomiRs based on synergetic signal amplification. *Biosens. Bioelectron.* **2020**, *159*, 112208. [[CrossRef](#)] [[PubMed](#)]
54. Liu, M.; Pan, B.; Tang, S.; Wang, W.; Hou, H.; Xie, B.; Liang, A.; Luo, A. A Label-Free Molecularly Imprinted Electrochemical Sensor Based on MXene Nanosheets Modified by Gold Nanoparticles for Sensitive and Selective Detection of Homocysteine. *J. Electrochem. Soc.* **2022**, *169*, 087503. [[CrossRef](#)]
55. Li, K.; Liang, M.; Wang, H.; Wang, X.; Huang, Y.; Coelho, J.; Pinilla, S.; Zhang, Y.; Qi, F.; Nicolosi, V.; et al. 3D MXene Architectures for Efficient Energy Storage and Conversion. *Adv. Funct. Mater.* **2020**, *30*, 2000842. [[CrossRef](#)]
56. Wen, X.-H.; Zhao, X.-F.; Peng, B.-F.; Yuan, K.-P.; Li, X.-X.; Zhu, L.-Y.; Lu, H.-L. Facile preparation of an electrochemical aptasensor based on Au NPs/graphene sponge for detection of homocysteine. *Appl. Surf. Sci.* **2021**, *556*, 149735. [[CrossRef](#)]
57. Idili, A.; Parolo, C.; Ortega, G.; Plaxco, K.W. Calibration-Free Measurement of Phenylalanine Levels in the Blood Using an Electrochemical Aptamer-Based Sensor Suitable for Point-of-Care Applications. *ACS Sens.* **2019**, *4*, 3227–3233. [[CrossRef](#)] [[PubMed](#)]
58. Sun, Z.; Jin, H.; Sun, Y.; Jiang, X.; Gui, R. Mn-Doping-induced hierarchical petal growth of a flower-like 3D MOF assembled with black phosphorous nanosheets as an electrochemical aptasensor of human stress-induced phosphoprotein 1. *Nanoscale* **2020**, *12*, 14538–14548. [[CrossRef](#)] [[PubMed](#)]
59. Zhang, L.; Li, Z.; Zhou, X.; Yang, G.; Yang, J.; Wang, H.; Wang, M.; Liang, C.; Wen, Y.; Lu, Y. Hybridization performance of DNA/mercaptohexanol mixed monolayers on electrodeposited nanoAu and rough Au surfaces. *J. Electroanal. Chem.* **2015**, *757*, 203–209. [[CrossRef](#)]
60. Lawrence, N.S.; Deo, R.P.; Wang, J. Detection of homocysteine at carbon nanotube paste electrodes. *Talanta* **2004**, *63*, 443–449. [[CrossRef](#)]
61. Beitollahi, H.; Zaimbashi, R.; Mahani, M.T.; Tajik, S. A label-free aptasensor for highly sensitive detection of homocysteine based on gold nanoparticles. *Bioelectrochemistry* **2020**, *134*, 107497. [[CrossRef](#)]
62. Neufeld, G.; Cohen, T.; Gengrinovitch, S.; Poltorak, Z. Vascular endothelial growth factor (VEGF) and its receptors. *FASEB J. Off. Publ. Fed. Am. Soc. Exp. Biol.* **1999**, *13*, 9–22. [[CrossRef](#)]
63. Sullivan, L.A.; Brekken, R.A. The VEGF family in cancer and antibody-based strategies for their inhibition. *MAbs* **2010**, *2*, 165–175. [[CrossRef](#)]
64. Aly, M.H.; Arafat, M.A.; Hussein, O.A.; Elsaid, H.H.; Abdel-Hammed, A.R. WITHDRAWN: Study of Angiopoietin-2 and vascular endothelial growth factor as markers of diabetic nephropathy onset in egyptians diabetic patients with non-albuminuric state. *Diabetes Metab. Syndr. Clin. Res. Rev.* **2019**, *13*, 1623–1627. [[CrossRef](#)] [[PubMed](#)]
65. Bozal-Palabiyik, B.; Lettieri, M.; Uslu, B.; Marrazza, G. Electrochemical Detection of Vascular Endothelial Growth Factor by Molecularly Imprinted Polymer. *Electroanalysis* **2019**, *31*, 1458–1464. [[CrossRef](#)]
66. Cheng, J.L.; Liu, X.P.; Chen, J.S.; Mao, C.J.; Jin, B.K. Highly sensitive electrochemiluminescence biosensor for VEGF(165) detection based on a g-C(3)N(4)/PDDA/CdSe nanocomposite. *Anal. Bioanal. Chem.* **2020**, *412*, 3073–3081. [[CrossRef](#)] [[PubMed](#)]
67. Harris, R.C. The Role of the Epidermal Growth Factor Receptor in Diabetic Kidney Disease. *Cells* **2022**, *11*, 3416. [[CrossRef](#)]
68. Li, N.; Nan, C.; Mei, X.; Sun, Y.; Feng, H.; Li, Y. Electrochemical sensor based on dual-template molecularly imprinted polymer and nanoporous gold leaf modified electrode for simultaneous determination of dopamine and uric acid. *Mikrochim. Acta.* **2020**, *187*, 496. [[CrossRef](#)]
69. Johari-Ahar, M.; Karami, P.; Ghanei, M.; Afkhami, A.; Bagheri, H. Development of a molecularly imprinted polymer tailored on disposable screen-printed electrodes for dual detection of EGFR and VEGF using nano-liposomal amplification strategy. *Biosens. Bioelectron.* **2018**, *107*, 26–33. [[CrossRef](#)]
70. Wang, J.-Y.; Xiao, L.; Wang, J.-Y. Posttranscriptional regulation of intestinal epithelial integrity by noncoding RNAs. *Wiley Interdiscip. Rev. RNA* **2017**, *8*, e1399. [[CrossRef](#)]
71. Wang, J.; Chen, J.; Sen, S. MicroRNA as Biomarkers and Diagnostics. *J. Cell Physiol.* **2016**, *231*, 25–30. [[CrossRef](#)]
72. Treiber, T.; Treiber, N.; Meister, G. Regulation of microRNA biogenesis and its crosstalk with other cellular pathways. *Nat. Rev. Mol. Cell Biol.* **2019**, *20*, 5–20. [[CrossRef](#)] [[PubMed](#)]
73. Trionfini, P.; Benigni, A.; Remuzzi, G. MicroRNAs in kidney physiology and disease. *Nat. Rev. Nephrol.* **2015**, *11*, 23–33. [[CrossRef](#)] [[PubMed](#)]

74. Parrizas, M.; Mundet, X.; Castano, C.; Canivell, S.; Cos, X.; Brugnara, L.; Giraldez-Garcia, C.; Regidor, E.; Mata-Cases, M.; Franch-Nadal, J.; et al. miR-10b and miR-223-3p in serum microvesicles signal progression from prediabetes to type 2 diabetes. *J. Endocrinol. Investig.* **2020**, *43*, 451–459. [[CrossRef](#)] [[PubMed](#)]
75. Liu, C.; Zhao, L.; Liang, D.; Zhang, X.; Song, W. An CuInS₂ photocathode for the sensitive photoelectrochemical determination of microRNA-21 based on DNA-protein interaction and exonuclease III assisted target recycling amplification. *Mikrochim. Acta.* **2019**, *186*, 692. [[CrossRef](#)]
76. Ma, Z.Y.; Ruan, Y.F.; Xu, F.; Zhao, W.W.; Xu, J.J.; Chen, H.Y. Protein Binding Bends the Gold Nanoparticle Capped DNA Sequence: Toward Novel Energy-Transfer-Based Photoelectrochemical Protein Detection. *Anal. Chem.* **2016**, *88*, 3864–3871. [[CrossRef](#)]
77. Takuma, N.; Mihoko, H.; Masafumi, K.; Seiki, I. Increased urinary excretions of immunoglobulin g, ceruloplasmin, and transferrin predict development of microalbuminuria in patients with type 2 diabetes. *Diabetes Care* **2006**, *29*, 142–144.
78. Narita, T.; Fujita, H.; Koshimura, J.; Meguro, H.; Kitazato, H.; Shimotomai, T.; Kagaya, E.; Suzuki, K.; Murata, M.; Usami, A.; et al. Glycemic control reverses increases in urinary excretions of immunoglobulin G and ceruloplasmin in type 2 diabetic patients with normoalbuminuria. *Horm. Metab. Res. Horm. Und Stoffwechselforschung Horm. Metab.* **2001**, *33*, 370–378. [[CrossRef](#)]
79. Yamazaki, M.; Ito, S.; Usami, A.; Tani, N.; Hanyu, O.; Nakagawa, O.; Nakamura, H.; Shibata, A. Urinary excretion rate of ceruloplasmin in non-insulin-dependent diabetic patients with different stages of nephropathy. *Eur. J. Endocrinol.* **1995**, *132*, 681–687. [[CrossRef](#)]
80. Haghshenas, E.; Madrakian, T.; Afkhami, A.; Saify Nabiabad, H. An electrochemical ceruloplasmin aptasensor using a glassy carbon electrode modified by diazonium-functionalized multiwalled carbon nanotubes. *J. Iran. Chem. Soc.* **2018**, *16*, 593–602. [[CrossRef](#)]
81. Ocana, C.; Hayat, A.; Mishra, R.K.; Vasilescu, A.; Del Valle, M.; Marty, J.L. Label free aptasensor for Lysozyme detection: A comparison of the analytical performance of two aptamers. *Bioelectrochemistry* **2015**, *105*, 72–77. [[CrossRef](#)]
82. Nancy, K.; Lipton, A. Platelets as a source of fibroblast growth-promoting activity. *Exp. Cell Res.* **1974**, *87*, 297–301.
83. Hongquan, Z.; Xing-Fang, L.; Chris, L.X. Differentiation and detection of PDGF isomers and their receptors by tunable aptamer capillary electrophoresis. *Anal. Chem.* **2009**, *81*, 7795–7800.
84. Pierce, G.F.; Tarpley, J.E.; Tseng, J.; Bready, J.; Chang, D.; Kenney, W.C.; Rudolph, R.; Robson, M.C.; Berg, J.V.; Reid, P. Detection of platelet-derived growth factor (PDGF)-AA in actively healing human wounds treated with recombinant PDGF-BB and absence of PDGF in chronic nonhealing wounds. *J. Clin. Investig.* **1995**, *96*, 1336–1350. [[CrossRef](#)] [[PubMed](#)]
85. Zhang, J.J.; Cao, J.T.; Shi, G.F.; Huang, K.J.; Liu, Y.M.; Ren, S.W. A luminol electrochemiluminescence aptasensor based on glucose oxidase modified gold nanoparticles for measurement of platelet-derived growth factor BB. *Talanta* **2015**, *132*, 65–71. [[CrossRef](#)] [[PubMed](#)]
86. Huang, K.J.; Liu, Y.J.; Zhang, J.Z.; Cao, J.T.; Liu, Y.M. Aptamer/Au nanoparticles/cobalt sulfide nanosheets biosensor for 17beta-estradiol detection using a guanine-rich complementary DNA sequence for signal amplification. *Biosens. Bioelectron.* **2015**, *67*, 184–191. [[CrossRef](#)]
87. Ge, Z.; Gu, H.; Li, Q.; Fan, C. Concept and Development of Framework Nucleic Acids. *J. Am. Chem. Soc.* **2018**, *140*, 17808–17819. [[CrossRef](#)]
88. Campuzano, S.; Yáñez-Sedeño, P.; Pingarrón, J.M. Tailoring Sensitivity in Electrochemical Nucleic Acid Hybridization Biosensing: Role of Surface Chemistry and Labeling Strategies. *ChemElectroChem* **2019**, *6*, 60–72. [[CrossRef](#)]
89. Ge, Z.; Fu, J.; Liu, M.; Jiang, S.; Andreoni, A.; Zuo, X.; Liu, Y.; Yan, H.; Fan, C. Constructing Submonolayer DNA Origami Scaffold on Gold Electrode for Wiring of Redox Enzymatic Cascade Pathways. *ACS Appl. Mater. Interfaces* **2019**, *11*, 13881–13887. [[CrossRef](#)]
90. Lu, N.; Pei, H.; Ge, Z.; Simmons, C.R.; Yan, H.; Fan, C. Charge transport within a three-dimensional DNA nanostructure framework. *J. Am. Chem. Soc.* **2012**, *134*, 13148–13151. [[CrossRef](#)]
91. Chen, X.; Zhou, G.; Song, P.; Wang, J.; Gao, J.; Lu, J.; Fan, C.; Zuo, X. Ultrasensitive electrochemical detection of prostate-specific antigen by using antibodies anchored on a DNA nanostructural scaffold. *Anal. Chem.* **2014**, *86*, 7337–7342. [[CrossRef](#)] [[PubMed](#)]
92. Huang, K.J.; Liu, Y.J.; Zhai, Q.F. Ultrasensitive biosensing platform based on layered vanadium disulfide-graphene composites coupling with tetrahedron-structured DNA probes and exonuclease III assisted signal amplification. *J. Mater. Chem. B* **2015**, *3*, 8180–8187. [[CrossRef](#)] [[PubMed](#)]
93. Ge, Z.; Lin, M.; Wang, P.; Pei, H.; Yan, J.; Shi, J.; Huang, Q.; He, D.; Fan, C.; Zuo, X. Hybridization Chain Reaction Amplification of MicroRNA Detection with a Tetrahedral DNA Nanostructure-Based Electrochemical Biosensor. *Anal. Chem.* **2014**, *86*, 2124–2130. [[CrossRef](#)] [[PubMed](#)]
94. Abi, A.; Lin, M.; Pei, H.; Fan, C.; Ferapontova, E.E.; Zuo, X. Electrochemical switching with 3D DNA tetrahedral nanostructures self-assembled at gold electrodes. *ACS Appl. Mater. Interfaces* **2014**, *6*, 8928–8931. [[CrossRef](#)] [[PubMed](#)]

Disclaimer/Publisher’s Note: The statements, opinions and data contained in all publications are solely those of the individual author(s) and contributor(s) and not of MDPI and/or the editor(s). MDPI and/or the editor(s) disclaim responsibility for any injury to people or property resulting from any ideas, methods, instructions or products referred to in the content.